

Exploration of Input Patterns for Enhancing the Performance of Liquid State Machines

Shasha Guo
National University of Defense
Technology
Changsha, China
guoshasha13@nudt.edu.cn

Lianhua Qu
National University of Defense
Technology
Changsha, China

Lei Wang
National University of Defense
Technology
Changsha, China
arrowya@gmail.com

Xulong Tang
University of Pittsburgh
Pittsburgh, USA

Shuo Tian
National University of Defense
Technology
Changsha, China

Shiming Li
National University of Defense
Technology
Changsha, China

Weixia Xu
National University of Defense
Technology
Changsha, China

Abstract

Spiking Neural Networks (SNN) have gain increasing attention for its low power consumption. But training SNN is challenging. Liquid State Machine (LSM), as a major type of Reservoir computing, has been widely recognized for its low training cost among SNNs. The exploration on LSM topology for enhancing performance often requires hyper-parameter search, which is both resource expensive and time consuming. We explore the influence of input scale reduction on LSM instead. There are two main reasons for studying input reduction of LSM. One is that input dimension of large images requires efficient processing. Another one is that input exploration is generally more economic than architecture search. To mitigate the difficulty in effectively dealing with huge input spaces of LSM, and to find that whether input reduction can enhance LSM performance, we explore several input patterns, namely fullscale, scanline, chessboard and patch. Several datasets have been used to evaluate the performance of the proposed input patterns, including two spatio image datasets and one spatio-temporal image database. The experimental results show that the reduced input under chessboard pattern improves the accuracy by up to 2%, and reduces execution time by up to 50% with up to 75% less input storage than the fullscale input pattern for LSM.

Keywords: LSM, encoding, input pattern

1 Introduction

In the past decades, both academia and industry have made great attempts to develop computing models to mimic brain function. While spiking neural networks

(SNNs) hold a lot of promise due to its closer resemblance to brains than older generations of artificial neural networks and are anticipated to be power efficient, the training of SNNs is nontrivial. There are several unsupervised learning algorithms, such as Winner-Take-All strategy [1] and spike-timing-dependent plasticity [2]. To develop supervised gradient-based training for SNNs, particularly recurrent SNNs, requires approximation to the neuron model and will consume large amounts of resources and training efforts.

There has been increasing interest in the concept of reservoir computing (RC). The liquid state machine (LSM) is one specific form of RC. LSM, first proposed by [3], has gained increasing popularity due to its lower training cost than other SNNs. It has been used for various applications such as image recognition [4, 5], movement prediction [6–8], decoding actual brain activity [9, 10], and speech recognition [11–13].

To find a LSM with the state-of-the-art results in real-world applications, many efforts of enhancing LSM focus on the exploration of LSM topology, such as self-organizing networks (SON) [14], small-world networks [15], deep LSM [5], and liquid ensembles [16]. These works either incur training algorithms or cost-intensive hyper-parameter search, which increase accuracy at the cost of performance or resource overhead.

There exist several approaches that could improve the accuracy of LSM without deviating from its inherent structure simplicity, like increasing the number of neurons in the liquid. However, this approach also demands more computations and storage. And the sensitivity of accuracy to neuron count decreases when the number of neurons exceeding a certain point [16].

Dealing with input is another issue that has significant impact on the performance of LSM. Some previous studies focus on the encoding methods of SNN input [17, 18]. [17] explores the encoding for rate coding of image input. [18] compares four temporal encoding method for converting analog values into spikes for SNN input. These two works focus on the encoding or converting method of analog real-values without considering the whole input size. With the increase in the size of images, the converted input size is also growing rapidly to a large scale. [19] uses a new method to encode images for SNN input. It utilizes the redundancy in images and sparsely encodes the images into spikes through certain "scanlines".

In this work, we aim to systematically explore the effect of reducing the input scale via input pattern on the performance of LSM, that is, accuracy, runtime and storage. There are two main reasons for this. First, the number of input pixels represents the number of input layer neurons. Large input processing is more time-consuming and resource-demanding than small input considering the same liquid architecture and synapse connection probability. Second, LSM performance not only refers to the accuracy, but also the storage and runtime. While previous work of parameter search mainly focus on the accuracy improvement, input pattern search takes consideration of these three aspects.

Our contributions of this paper are as follows:

- We explore several input patterns for LSM simulation, and compare their performance in accuracy, execution time and input storage cost. We use three datasets, including two frame-based datasets and one spatio-temporal event-based dataset.
- We propose two algorithms for using different input patterns to generate desired spike trains from frame-based datasets and event-based database.
- We use several readout layers to show that the effects brought by input patterns are reliable, i.e., the performance change of LSM is indeed brought by the input pattern.

We validate our idea on several benchmarks including two frame-based datasets and one event-based neuromorphic dataset. The frame-based datasets are converted to spiking format as input of LSM. The experimental results show that the reduced input under chessboard pattern can improve the accuracy by up to 2%, and reduces the execution time by up to 50% with up to 75% less input storage than fullscale pattern for LSM.

2 Preliminaries

2.1 LSM

A liquid state machine (as shown in Figure 1) consists of three main components: an input layer, a liquid layer

and a readout layer. Input is fed through the input layer into the liquid. The liquid receives the input streams and transforms them into non-linear patterns in higher dimensions, which acts as a filter. The state vector of the liquid is then used for analysis and interpretation by the readout layer, which consists of either memroyless artificial neurons or spiking neurons.

A liquid neuron can be either excitatory (E) or inhibitory (I) according how it affects other neurons. Neurons are connected by synapses, and the weight on a synapse represents how much the pre-synaptic neuron's activity affects the post-synaptic neuron. The connections between two neurons in the liquids are arranged with probability C . C depends on the type of pre-synaptic and the post-synaptic neurons, that is whether they are the excitatory or inhibitory cells.

2.2 Neuron Model

In our experiments, we use the standard leaky-integrate-and-fire (LIF) neuron model [20] to mimic the dynamics of both excitatory and inhibitory spiking neurons. The LIF model is probably one of the most popular spiking neuron models, more biologically realistic than the IF model [21]. A LIF neuron fires a spike when the membrane potential (v) reaches the threshold value (v_{th}). After spiking, the membrane potential is reset to the resting value. The dynamics of the membrane potential of the LIF neuron can be described as follows: $\tau_m \frac{dv}{dt} = -v(t) + RI(t)$. $I(t)$ is input current, τ_m is the membrane time-constant, and R is the membrane resistance. The formulations elaborated in [22] are used for modeling the dynamics of the LIF neurons in this paper.

2.3 Image to Spike Conversion

In general, SNNs receive and process event-driven spike signals. Thus, the conversion to spike trains is needed when testing SNNs over frame-based datasets in real value. One of the prevalent strategies is the probabilistic sampling. At every time step, it samples the original pixel intensity (usually normalized to $[0, 1]$) into a binary value, wherein the probability of being 1 (firing a spike) equals to the intensity value. The sampling follows a given probability distribution such as Bernoulli distribution or Poisson distribution.

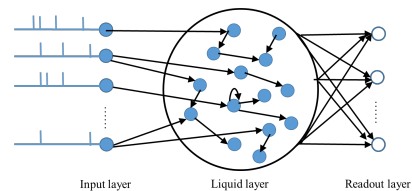


Figure 1. Illustration of LSM.

2.4 Training Readout Layer

We use two algorithms for readout layer training, back propagation algorithm (BP) [23] with stochastic gradient descent (SGD), and state vector machine (SVM) [24]. The reason of using several classifiers is that we want to explore whether certain input pattern can bring similar effects despite using different readouts.

The readout layer takes the normalized liquid state vectors as input. The liquid state vectors record the firing number of each neuron for all input images during the simulation, which are then normalized by the most spiking numbers in order to range between 0 and 1.

When using SVM as the readout layer, we add some aggressive operations on the normalized state vectors before inputted into the SVM via a binarization function. If the element exceeds 0.5, the value will be set as 1. Otherwise, it will be set to 0. This is SVM1. The SVM without the binarization step is called SVM2.

3 Method

To reduce the difficulty in effectively processing huge input spaces of LSM, we explore the influence of dimension reduction in input layer on LSM performance.

We explore four input patterns, namely, fullscale, scanline, chessboard, and patch. Fullscale pattern is the baseline, i.e., using all pixels of an image as input. Scanline pattern is used in [19] (shown in Figure 2(a)) as an encoder for images. It is inspired by human saccadic eye movements.

The last two input patterns, chessboard and patch, are inspired by two conventional computer vision techniques: template matching and keypoint detection for feature detection and matching. Examples of the two techniques are shown in Figure 3. They were used to solve computer vision tasks before the era of artificial neural networks. This reveals that some parts of an image are able to show the significant features for recognition and classification. To reduce the computation cost, we select the pixels and small patches evenly, rather than the way that first computes the importance of the pixels or patches based on some algorithms and then chooses them according to the importance. As shown in Figure 2(b) and Figure 2(c), our approach requires little computing to see whether such simple patterns could have good performance on LSM.

Given that there are four input patterns, we need a universal method to generate corresponding spike trains when applying different input patterns on the same dataset. As frame-based databases and event-based dataset store data in different formats, i.e., images and spike trains, we propose two algorithms, algorithm 1

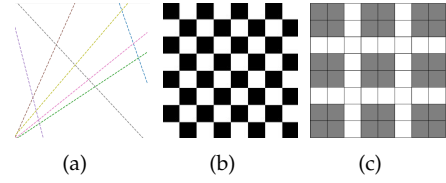


Figure 2. Example of different input patterns. (a) Scanline. (b) Chessboard. (c) Patch.

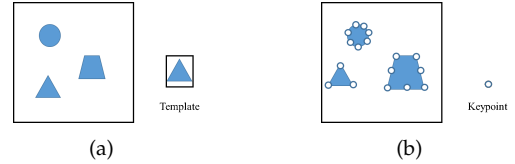


Figure 3. Techniques for feature detection and matching. (a) Template matching. (b) Keypoint detection.

Algorithm 1 Algorithm for frame-based dataset

Input: input pattern p
 $(p \in \{fullscale, scanline, chessboard, patch\})$,
simulation time: T , desired spike train number: N_1 , target set: X
(training or testing), number of samples in X : N_2 , image height: H ,
image width: W

Output: spike train index list: SL , spike train time list: TL

- 1: generate fixed pixel id list L based on the input pattern and the size of images in X
- 2: initialize a monitor M in BRIAN to record the neuron index and time when a spike occurs
- 3: **for** $i = 0$ to N_1 **do**
- 4: generate an empty list R as rate list
- 5: get an image matrix from X indexed by $(i\%N_2)$
- 6: **for** j in L **do**
- 7: get the activation value a of pixel j in the image
- 8: put a into rate list R
- 9: **end for**
- 10: generate Poisson spike trains based on the rate list R in BRIAN
- 11: **end for**
- 12: get SL and TL from M
- 13: **return** SL and TL

and algorithm 2, to get the desired spike trains for frame-based datasets and event-based dataset respectively. **The algorithms are applicable for all input patterns.**

4 Experiment Setup

We use two LSM architectures and three datasets in this work. The liquid was modeled in BRIAN2 [25], a Python-based spiking neural network simulator.

The experimental settings of the two architecture on the three datasets are listed in Table 1.

Algorithm 2 Algorithm for event-based dataset

Input: input pattern p
 $(p \in \{fullscale, scanline, chessboard, patch\})$,
simulation time: T , target set: X (training or testing), image
height: H , image width: W

Output: spike train index list: SL , spike train time list: TL

- 1: generate fixed pixel id list L based on input pattern p , H and W .
- 2: sample spike records in X within time T and get four lists P_{ON} , P_{OFF} , T_{ON} and T_{OFF} .
- 3: $N = H \times W$
- 4: generate two empty lists DL_{ON} and DL_{OFF} as indices list to be deleted from the above lists.
- 5: **for** $i = 0$ to N **do**
- 6: **if** $(i \notin L)$ **then**
- 7: find the indices at which the P_{ON} equals to i and put these indices into DL_{ON} ;
- 8: update DL_{OFF} as above.
- 9: **end if**
- 10: **end for**
- 11: delete elements indexed by DL_{ON} from P_{ON} and T_{ON} ; delete elements indexed by DL_{OFF} from P_{OFF} and T_{OFF}
- 12: **return** P_{ON} , T_{ON} , P_{OFF} and T_{OFF}



Figure 4. Example of N-MNIST dataset [27]. The two colors represent two event types: ON and OFF.

4.1 Benchmark Datasets

MNIST [26] dataset is commonly used in machine learning applications in computer vision. MNIST has 60000 images for training and 10000 other images for testing. Each digit frame is a 28×28 grayscale image.

N-MNIST [27] is the spike version of the original MNIST dataset, which also contains 60,000 training samples and 10 000 testing samples. Each sample in N-MNIST is a spatio-temporal spike pattern with size of $34 \times 34 \times 2 \times T$, where T is the recording time length. An example of N-MNIST is shown in Figure 4. **We use a subset of MNIST and NMNIST for experiments.**

We also make use of the JAFFE [28] dataset, which contains 213 images of female facial expressions posed by 10 Japanese women, grouped into 7 classes. We use two image representations of JAFFE, by resizing and cropping the images to re-center the eyes, nose, and mouth appear in the picture. One representation contains a small part of the face (10×45 pixels) as same as the the size in [4]. The other representation contains 45×45 pixels. Examples are presented in Figure 5.

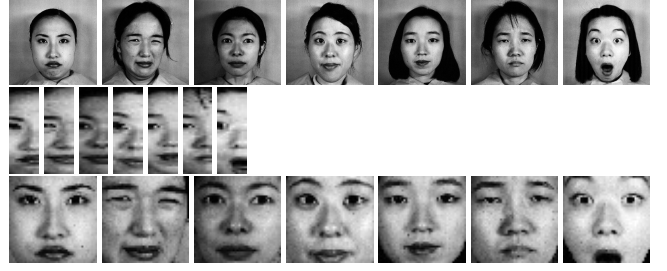


Figure 5. Examples of JAFFE dataset under different representations. The upper line shows the original grayscale images with 256×256 pixels, the middle line shows the representation with 10×45 pixels and the bottom line shows the other representation with 45×45 pixels. The facial expression from left to right is anger, disgust, fear, happy, neutral, sadness and surprise.

Table 1. Experimental Settings.

Dataset	Pattern	Arch	Num	Train Samples	Test Samples
MNIST	All	1RC, 5RC	1000	10000	10000
N-MNIST	FS, CB	1RC, 5RC	1000	10000	10000
JAFFE1 ^a	FS, SL, CB	1RC	450	1000	100
JAFFE2 ^b	FS, SL, CB	1RC	1350	1000	100

^aJAFFE1 refers to the representation of 10×45 pixels.

^bJAFFE2 refers to the representation of 45×45 pixels.

FS is fullscale, SL is scanline, CB is chessboard and PA means Patch. The column *Num* means the total number of neurons in the reservoir.

4.2 Architectures

We use two LSM architectures here. One architecture contains a single liquid, which is called 1RC for simplicity. Another architecture is denoted as 5RC, which consists of five liquids in parallel like in [16]. The total number of neurons in the five liquids will be as same as that in the 1RC for a fair comparison.

All synapse weights, i.e., input-to-liquid, liquid-to-liquid, and liquid-to-readout weights, are initialized from a Gaussian distribution of mean 0.5 and variance 0.16. All the hyper-parameters are listed in Table 2.

5 Experiment results

The fullscale pattern is regarded as baseline. We used a more aggressive chessboard pattern than Figure 2(b) shows. It only samples 1/4 of the fullscale pixels.

5.1 Accuracy

We repeat the simulation and training process several times and only the best results are listed for further discussions of MNIST and N-MNIST. For JAFFE we adopt other mechanisms (introduced in section 5.1.3).

Table 2. Hyper-parameters Value.

	C_{EE}	C_{EI}	C_{IE}	C_{II}	IR	OR	EIR
(N-)MNIST	0.4	0.4	0.5	0	0.2	0.9	0.8
JAFFE1/2	0.3	0.2	0.4	0.1	0.1/0.05		

(N-)MNIST represents MNIST and N-MNIST. C_{EE} is the connection probability of any two excitatory neurons in the liquid, and C_{EI} is the connection probability from an excitatory neuron to an inhibitory neuron. EIR represents the percentage of excitatory neurons in the liquid, IR is the ratio of connections between input layer neurons and the excitatory liquid neurons, OR is the ratio of connections between excitatory liquid neurons and readout layer neurons.

5.1.1 MNIST. Table 3 reveals the performance of LSM on MNIST dataset using four different input patterns and three classifiers. For training, fullscale pattern always yields the best accuracy. For testing, it can be seen that for 1RC, chessboard pattern brings the best testing accuracy, 0.5% higher than fullscale pattern. And for 5RC, the difference between fullscale and chessboard pattern are less than 0.3%. Other two patterns are about 2% to 4% worse than fullscale and chessboard.

In addition, we can see that for all readout methods, the accuracy values of chessboard pattern are similar with those of fullscale pattern and over-perform other two patterns. This shows that the effects brought by input patterns are reliable. And as the SGD method generally performs better than SVM methods, we decide to use SGD classifier for further investigations.

Table 3. Accuracy Comparison on MNIST Dataset.

		1RC		5RC			
		SGD	SVM1	SVM2	SGD	SVM1	SVM2
Train	FS	93.90%	74.01%	86.31%	94.09%	92.39%	90.91%
	SL	90.64%	69.13%	81.17%	89.42%	90.42%	86.81%
	CB	92.30%	72.04%	84.46%	93.06%	91.57%	89.69%
	PA	89.93%	70.73%	80.65%	89.34%	88.02%	85.48%
Test	FS	88.73%	72.24%	85.28%	89.62%	89.52%	89.56%
	SL	86.37%	66.79%	79.93%	85.39%	86.79%	85.52%
	CB	89.39%	71.61%	84.36%	89.35%	89.34%	89.27%
	PA	86.58%	68.58%	79.61%	86.51%	85.15%	85.14%

FS is fullscale, SL is scanline, CB is chessboard and PA means Patch.

5.1.2 N-MNIST. We train LSM on both channels, i.e., ON and OFF. Table 4 shows the accuracy comparison of LSM on N-MNIST dataset using SGD for readout layer training. The nearly 10% differences between training and testing set show that this classifier is over-fitting. It's worth noticing that chessboard pattern is beneficial to mitigate this effect. This is reasonable, as less input is suggested to avoid over-fitting. For inference, with 1RC architecture, using chessboard pattern achieves nearly 5% higher accuracy than using fullscale pattern.

Table 4. Accuracy Comparison on N-MNIST Dataset.

	Train		Test	
	fullscale	chessboard	fullscale	chessboard
1RC	98.52%	99.42%	86.69%	91.67%
5RC	98.94%	97.71%	87.49%	89.14%

Table 5. Testing Accuracy Comparison on JAFFE.

No.	JAFFE1			JAFFE2		
	FS	SL	CB	FS	SL	CB
1	47.00%	43.00%	49.00%	62.00%	58.00%	61.00%
2	43.00%	39.00%	50.00%	54.00%	53.00%	53.00%
3	50.00%	55.00%	51.00%	64.00%	57.00%	58.00%
4	29.00%	21.00%	38.00%	76.00%	56.00%	69.00%
5	27.00%	27.00%	22.00%	54.00%	54.00%	53.00%
6	29.00%	32.00%	31.00%	68.00%	57.00%	67.00%
7	48.00%	45.00%	53.00%	64.00%	53.00%	52.00%
8	48.00%	51.00%	44.00%	60.00%	60.00%	65.00%
9	54.00%	51.00%	55.00%	66.00%	53.00%	64.00%
10	42.00%	55.00%	49.00%	63.00%	58.00%	59.00%
AVG	41.70%	41.90%	44.20%	63.10%	55.90%	60.10%

FS means fullscale, SL means scanline, and CB means chessboard.

With 5RC architecture, the difference between the two patterns is not significant, but still, chessboard pattern is 1.65% better than fullscale pattern.

5.1.3 JAFFE. Since the size of the JAFFE database is limited, we use two methods to enhance the validation. First, we use 10-fold cross-validation technique. Second, we generate desired number of spike train samples by repeating the limited images.

Table 5 shows the inference accuracy of LSM on JAFFE using fullscale, scanline and chessboard pattern. The last line is the average accuracy derived from the ten-fold cross validation. It can be seen that chessboard pattern is still competitive with fullscale pattern, with about $\pm 3\%$ in accuracy. However, scanline performs much worse than the fullscale pattern on JAFFE2, with up to 7% decrease in accuracy. The number of pixels from scanline pattern is similar to that from chessboard. Therefore, it could take several runs for randomly generating a set of scanlines that contain proper pixels and yield good performance. In other words, the performance will be worse if the scanlines are not properly chosen.

5.2 Storage

For storage, we refer to the input storage, i.e., spike records either generated from frame-based dataset or sampled from event-based dataset for training and testing, rather than the liquid state vector or the connection weights. The reason for storing input spike records is

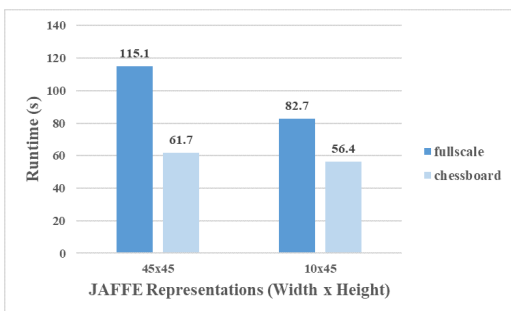


Figure 6. Average Runtime comparison on JAFFE.

that we want to feed the whole training samples into SNN framework at once rather than generating the spike trains for each sample one by one at simulation. The one-time feeding method greatly improve the learning efficiency and reduce the whole processing time [29]. The reduction in input storage by other input patterns compared with the fullscale pattern is obvious. With the same simulation time length per record, the reduction is proportional to the decrease in the number of input pixels. For instance, the number of pixels from chessboard pattern is only a quarter of that from fullscale pattern. So is the size of the spike records for training and testing, which is a 75% reduction in input storage.

5.3 Time

Figure 6 shows the runtime cost of using fullscale and chessboard pattern on JAFFE1 and JAFFE2. The figure is derived from averaging the result of ten simulations. It is not as expected to reduce as much as the input storage. But nearly 30% to 50% reduction in runtime is also impressive. We find similar data in other experiments.

6 Conclusion

Liquid state machine (LSM) gets increasing popularity for it has less difficulty in training than other spiking neural networks. There are many efforts for enhancing LSM performance. For example, many works focus on exploring topology variety of LSM or enlarging the number of neurons in the liquid. These incurs computing and/or storage overhead. Large input space of LSM is also a factor that influence the LSM performance. We explore the influence of the reduction in input scale on LSM performance in this work via different input patterns. Using several input patterns and benchmark datasets, we show that input size reduction according to a certain input pattern can indeed have positive influence on the LSM performance with respect to accuracy, storage cost, and runtime. The best input pattern we discover is the chessboard pattern that can achieve nearly

the same or better accuracy (2% increase) at most occasions on frame-based datasets as well as the event-based dataset. At the same time, it can achieve up to 75% input storage reduction and consumes only 50% runtime in the best case. From the observations, we conclude that input size reduction is a good technique for saving computing and storage resource while keeping the same accuracy for real-world applications of LSM. And it can be integrated with variations of LSM architecture like the ensembles of small liquids. In the future, we will further explore how LSM will react to changes in input, like more complex input pattern, and validate it on more temporal datasets.

References

- [1] Shuai Li, Bo Liu, and Yangming Li. Selective positive-negative feedback produces the winner-take-all competition in recurrent neural networks. *IEEE transactions on neural networks and learning systems*, 24(2):301–309, 2012.
- [2] Timothée Masquelier and Simon J Thorpe. Unsupervised learning of visual features through spike timing dependent plasticity. *PLoS computational biology*, 3(2), 2007.
- [3] Wolfgang Maass, Thomas Natschläger, and Henry Markram. Real-time computing without stable states: A new framework for neural computation based on perturbations. *Neural computation*, 14(11):2531–2560, 2002.
- [4] Beata J Grzyb, Eris Chinellato, Grzegorz M Wojcik, and Wieslaw A Kaminski. Facial expression recognition based on liquid state machines built of alternative neuron models. In *2009 International Joint Conference on Neural Networks*, pages 1011–1017. IEEE, 2009.
- [5] Qian Wang and Peng Li. D-lsm: Deep liquid state machine with unsupervised recurrent reservoir tuning. In *2016 23rd International Conference on Pattern Recognition (ICPR)*, pages 2652–2657. IEEE, 2016.
- [6] Wolfgang Maass, Robert Legenstein, and Henry Markram. A new approach towards vision suggested by biologically realistic neural microcircuit models. In *International Workshop on Biologically Motivated Computer Vision*, pages 282–293. Springer, 2002.
- [7] Harald Burgsteiner, Mark Kröll, Alexander Leopold, and Gerald Steinbauer. Movement prediction from real-world images using a liquid state machine. *Applied Intelligence*, 26(2):99–109, 2007.
- [8] Jacques Kaiser, Rainer Stal, Anand Subramoney, Arne Roennau, and Rüdiger Dillmann. Scaling up liquid state machines to predict over address events from dynamic vision sensors. *Bioinspiration & biomimetics*, 12(5):055001, 2017.
- [9] Danko Nikolić, Stefan Häusler, Wolf Singer, and Wolfgang Maass. Distributed fading memory for stimulus properties in the primary visual cortex. *PLoS biology*, 7(12), 2009.
- [10] Obada Al Zoubi, Mariette Awad, and Nikola K Kasabov. Any-time multipurpose emotion recognition from eeg data using a liquid state machine based framework. *Artificial intelligence in medicine*, 86:1–8, 2018.
- [11] Yong Zhang, Peng Li, Yingyezhe Jin, and Yoonsuck Choe. A digital liquid state machine with biologically inspired learning and its application to speech recognition. *IEEE transactions on neural networks and learning systems*, 26(11):2635–2649, 2015.
- [12] Yingyezhe Jin and Peng Li. Performance and robustness of bio-inspired digital liquid state machines: A case study of speech recognition. *Neurocomputing*, 226:145–160, 2017.

- [13] Wenrui Zhang and Peng Li. Information-theoretic intrinsic plasticity for online unsupervised learning in spiking neural networks. *Frontiers in neuroscience*, 13, 2019.
- [14] Shengyuan Luo, Hang Guan, Xiumin Li, Fangzheng Xue, and Hongjun Zhou. Improving liquid state machine in temporal pattern classification. In *2018 15th International Conference on Control, Automation, Robotics and Vision (ICARCV)*, pages 88–91. IEEE, 2018.
- [15] Hananel Hazan and Larry M Manevitz. Topological constraints and robustness in liquid state machines. *Expert Systems with Applications*, 39(2):1597–1606, 2012.
- [16] Parami Wijesinghe, Gopalakrishnan Srinivasan, Priyadarshini Panda, and Kaushik Roy. Analysis of liquid ensembles for enhancing the performance and accuracy of liquid state machines. *Frontiers in neuroscience*, 13:504, 2019.
- [17] Yang Xu, Huajin Tang, Jinwei Xing, and Hongying Li. Spike trains encoding and threshold rescaling method for deep spiking neural networks. In *2017 IEEE Symposium Series on Computational Intelligence (SSCI)*, pages 1–6. IEEE, 2017.
- [18] Balint Petro, Nikola Kasabov, and Rita M Kiss. Selection and optimization of temporal spike encoding methods for spiking neural networks. *IEEE transactions on neural networks and learning systems*, 2019.
- [19] Chit-Kwan Lin, Andreas Wild, Gautham N Chinya, Yongqiang Cao, Mike Davies, Daniel M Lavery, and Hong Wang. Programming spiking neural networks on intel's Loihi. *Computer*, 51(3):52–61, 2018.
- [20] Wulfram Gerstner and Werner M Kistler. *Spiking neuron models: Single neurons, populations, plasticity*. Cambridge university press, 2002.
- [21] Christof Koch. *Biophysics of computation: information processing in single neurons*. Oxford university press, 2004.
- [22] Peter U Diehl and Matthew Cook. Unsupervised learning of digit recognition using spike-timing-dependent plasticity. *Frontiers in computational neuroscience*, 9:99, 2015.
- [23] David E Rumelhart, Geoffrey E Hinton, and Ronald J Williams. Learning representations by back-propagating errors. *nature*, 323(6088):533–536, 1986.
- [24] Corinna Cortes and Vladimir Vapnik. Support-vector networks. *Machine learning*, 20(3):273–297, 1995.
- [25] Marcel Stimberg, Romain Brette, and Dan FM Goodman. Brian 2, an intuitive and efficient neural simulator. *Elife*, 8, 2019.
- [26] Yann LeCun, Léon Bottou, Yoshua Bengio, and Patrick Haffner. Gradient-based learning applied to document recognition. *Proceedings of the IEEE*, 86(11):2278–2324, 1998.
- [27] Garrick Orchard, Ajinkya Jayawant, Gregory K Cohen, and Nitish Thakor. Converting static image datasets to spiking neuro-morphic datasets using saccades. *Frontiers in neuroscience*, 9:437, 2015.
- [28] Michael Lyons, Shigeru Akamatsu, Miyuki Kamachi, and Jiro Gyoba. Coding facial expressions with gabor wavelets. In *Proceedings Third IEEE international conference on automatic face and gesture recognition*, pages 200–205. IEEE, 1998.
- [29] Daqi Liu and Shigang Yue. Event-driven continuous stdp learning with deep structure for visual pattern recognition. *IEEE transactions on cybernetics*, 49(4):1377–1390, 2018.